Journal of Solid State Chemistry 186 (2012) 268–277

Contents lists available at SciVerse ScienceDirect

Journal of Solid State Chemistry

journal homepage: www.elsevier.com/locate/jssc

Growth conditions, structure, Raman characterization and optical properties of Sm-doped $(Lu_xGd_{1-x})_2SiO_5$ single crystals grown by the Czochralski method

Michał Głowacki [a,*], Grażyna Dominiak-Dzik [b], Witold Ryba-Romanowski [b], Radosław Lisiecki [b], Adam Strzęp [b], Tomasz Runka [c], Mirosław Drozdowski [c], Viktor Domukhovski [a], Ryszard Diduszko [a,d], Marek Berkowski [a]

[a] Institute of Physics, Polish Academy of Sciences, Al. Lotników 32/46, 02-668 Warsaw, Poland
[b] Institute of Low Temperature and Structure Research, Polish Academy of Sciences, ul. Okólna 2, 50-950 Wrocław, Poland
[c] Faculty of Technical Physics, Poznan University of Technology, ul. Nieszawska 13A, 60-965 Poznan, Poland
[d] Institute of Electronic Materials Technology, ul. Wolczynska 133, 01-919 Warsaw, Poland

ARTICLE INFO

Article history:
Received 6 November 2011
Received in revised form
14 December 2011
Accepted 15 December 2011
Available online 24 December 2011

Keywords:
Rare-earth orthosilicates solid solution
Single crystal structure
X-ray powder diffraction
Optical studies
Raman

ABSTRACT

The $(Lu_xGd_{0.995-x}Sm_{0.005})_2SiO_5$ single crystals with $x=0.095$, 0.11, 0.15, 0.17, 0.19 0.35 and 0.5 were grown by the Czochralski method. Structural properties were investigated by X-ray diffraction measurements. Unit cell parameters and cell volume were determined by the Rietveld refinement of the collected X-ray powder spectra. The segregation features between Gd and Lu were estimated and analyzed. Vibrational properties of the solid solutions were analyzed on the basis of polarized Raman spectra acquired at 300–875 K temperature range. Absorption and emission spectra of Sm^{3+} ion in the crystals with different composition were analyzed in the terms of dopant energy levels, oscillator strengths of transitions and spectral features of luminescence bands in the visible range. Both structural and optical investigations revealed that change of Lu^{3+} content in $(Lu_xGd_{0.995-x}Sm_{0.005})_2SiO_5$ solid solution crystals induces the phase transition from $C2/c$ (Lu_2SiO_5) to $P2_1/c$ (Gd_2SiO_5) structure. It was found that the break of LSO to GSO-type structure occurs at $0.15 < x < 0.17$.

1. Introduction

Rare earth oxyorthosilicates with stoichiometric formula Re_2SiO_5 belong to two different types of monoclinic structure that are determined by a radius of rare earth ion. Representatives of both crystal types are gadolinium silicate Gd_2SiO_5 (GSO) with the $P2_1/c$ space group and lutetium silicate Lu_2SiO_5 (LSO) or yttrium silicate Y_2SiO_5 (YSO) described by $C2/c$ one [1,2]. LSO crystals doped with Ce^{3+} owing to unique thermal and optical properties offer applications as scintillation detectors for positron emission tomography (PET) and new efficient phosphors [3–6]. Both LSO and GSO possess a great ability to accommodate rare earth ions; doped with Dy^{3+} or Sm^{3+} can be promising systems for applications as white-light emitters owing to an intense luminescence in the blue and yellow spectral range. Also efficient laser action at around 1 μm was reported for the Yb:LSO crystal [7]. A large isomorphic capacity of lattices with monoclinic space symmetry opens the possibility for obtaining solid solutions by substitution of one rare earth element by another.

A technological interest in the $(Lu_xGd_{1-x})_2SiO_5$ (LGSO) solid solution crystals doped with rare earth ions (mainly Ce^{3+}) has been focused on the reducing the melting temperature of those promising scintillating materials [8]. The melting point of LSO is very close to the breakdown of iridium crucible and heat insulation made of stabilized zirconia ceramics. Lowering the melting temperature of the material also allows to safely increase axial temperature gradients at the crystal–melt interface in order to counteract the influence of expected segregation of both the host components and dopant. Another benefit of the LGSO over LSO crystals is a price reduction of starting materials due to replacing large amount (over 80 at.%) of expensive Lu_2O_3 by much cheaper Gd_2O_3 oxide. A practical aspect of lutetium substitution by gadolinium in the orthosilicate matrix has been reported by Sidletskiy et al. [9] which suggested that such substitution effectively reduces the difference between the ionic radius of dopants (Gd^{3+}, RE^{3+}) and Lu^{3+} ions building the LSO matrix, especially when dopant ion is one of rare earths with large ionic radius, such as Ce^{3+}, Pr^{3+}, etc. It is advantageous to crystalline material due to the more homogeneous distribution of dopant in

* Corresponding author.
E-mail address: glowacki@ifpan.edu.pl (M. Głowacki).

0022-4596/$ - see front matter © 2011 Elsevier Inc. All rights reserved.
doi:10.1016/j.jssc.2011.12.021

the matrix as well as to smaller dopant segregation. With a large difference in ionic radii, the distribution coefficient is much less than unity ($k \ll 1$). Thus, the replacing a substantial part of Lu^{3+} ions for Gd^{3+} ones, without changing the structure from C2/c (LSO) to P2$_1$/c (GSO) [9,10] is beneficial in every aspect; lower melting point, more homogeneous distribution of dopant in crystal host, and a smaller dopant segregation. It should be noted here that gadolinium orthosilicate crystal GSO exhibits the tendency to crack during the crystallization process and further treatments. A partial replacement of gadolinium by lutetium in GSO, significantly reduces stress in obtained LGSO solid solution. Moreover, the LGSO single crystal possesses a better plasticity and lower tendency to crack than the GSO one. Problem of the dopant segregation in rare earth orthosilicates was considered in several works in past years. Brandle et al. [11] have reported results of doping GSO with Tb^{3+} and Yb^{3+} and YSO with Ce^{3+}, Pr^{3+}, Nd^{3+}, Sm^{3+}, Gd^{3+}, Tb^{3+} (ions larger than Y^{3+}) as well as with Er^{3+}, Tm^{3+} and Yb^{3+} (ions smaller than Y^{3+}). On the basis of obtained results, they concluded that ionic radius of dopant strongly affects its segregation coefficient k_{eff} in the GSO and YSO hosts.; $k_{eff} < 1$ and $k_{eff} > 1$ were determined for dopant ions larger and smaller than Gd^{3+} and Y^{3+}, respectively. Similar observations were reported for the GSO:Ce, YSO:Ce and LSO:Ce systems [12] or for the LSO–GSO solid solution doped with 0.2 at.% Ce [8].

This work is aimed at the study of structural and optical properties of $(Lu_xGd_{0.995-x}Sm_{0.005})_2SiO_5$ (LGSO:Sm) solid solution crystal with different Lu/Gd ratio that were grown by the Czochralski technique. The special emphasis was put on determining the Lu/Gd composition ratio (as exactly as possible) being an essential for the change of crystal structure reported for LGSO solid solution crystal. Structural and physical results like space group, unit cell parameters, cell volume and melting temperatures were combined with those obtained for Dy-doped the LSO, GSO and LGSO hosts and reported in our previously papers [10,13,14]. Optical studies (Raman spectra of LGSO:Sm as well as samarium absorption, luminescence and dynamics of luminescent state) were examined and analyzed in the aspect of structural changes.

2. Material and methods

Solid solution single crystals of $(Lu_xGd_{0.995-x}Sm_{0.005})_2SiO_5$ with nominal values of $x=0.095$, 0.11, 0.15, 0.17, 0.19 0.35 and 0.5 were grown by the Czochralski method in an inductively heated iridium crucible under the nitrogen atmosphere. As starting materials the following oxides were used: Gd_2O_3 (5N purity), Lu_2O_3 (4N), Sm_2O_3 (5N) and SiO_2 (4N5). They were fired at 1000 °C for 4 h before weighing and mixing. Stoichiometric mixtures of powders were pressed into cylinder tablets under a high pressure (200 MPa). The tablets were sintered in a furnace at 1500 °C for 6 h before they were loaded into a crucible. Single crystals were grown with a convex crystal melt interface on an iridium 2 mm rod with a pulling rate of 1.5–2 mm/h and a speed of rotation of 20 rpm. Transparent and almost colorless crystals with 20 mm of the diameter were grown from the 40 mm crucible. The plates with orientations (1 0 0) and (0 1 0) and thickness of 4 mm were cut from the crystals with nominal value of $x=0.15$, 0.17, 0.19, 0.5 and used in optical measurements. Samples for Raman measurements were cut from the crystals with nominal value of $x=0.15$ and 0.17. A strong tendency to crack parallel to the cleavage plane (1 0 0) was observed especially for samples cut from crystals with $x \leq 0.15$.

Phase analysis and structural refinement were performed on powdered samples with a Siemens D5000 diffractometer (Ni-filtered CuKα radiation). Data were collected in the range 20–100° with a step of 0.02° and averaging time of 10 s/step. The powder diffraction patterns were analyzed by the Rietveld refinement method using DBWS-9807 program [15].

The chemical composition of LGSO:Sm single crystals was checked by Field Emission Scanning Electron Microscopy (FESEM) JEOL JSM-7600F operating at 20 kV incident energy and coupled to Oxford INCA Energy Dispersive X-ray (EDX) spectroscope.

Polarized Raman spectra of two oriented LGSO:Sm crystals were recorded in different scattering configurations using Renishaw InVia Raman microscope equipped with a thermoelectrically (TE)-cooled CCD detector and an Ar^+ ion laser working at 488 and 514.5 nm wavelengths. In preliminary measurements, both laser lines were used for excitation the samples. However, due to appearing the luminescence background in the range of Raman measurements, the 514.5 nm laser line was used, as a better choice, for proper measurements. The laser power at the focus spot (about 1 μm in diameter) was kept below 1 mW. The spectra were measured in the 70–1100 cm^{-1} range with the spectral resolution better than 2 cm^{-1}. Temperature measurements were performed using Linkam THMS 600 cooling/heating stage in the 300–875 K temperature range.

Unpolarized optical measurements were carried out at 300 K. Absorption spectra were recorded with a Varian 5E UV–vis-NIR spectrophotometer. High-resolution luminescence measurements were carried out using an Optron Dong Woo Fluorometer System containing ozone-free Xe lamp as an excitation source.

3. Results and discussion

3.1. Structure and phase transition.

Table 1 presents nominal and real compositions of $(Lu_xGd_{0.995-x}Sm_{0.005})_2SiO_5$ and values of segregation coefficients between gadolinium and lutetium ($k_{effGd/Lu}$) in the LGSO:Sm

Table 1
Chemical Composition of Melt and Solid Solution Crystal doped with Sm^{3+}, and Effective Segregation Coefficients between Gadolinium and Lutetium $k_{eff\ Gd/Lu}$. For Comparison, the Data reported for LGSO:Dy [10] and LGSO:Ce [8] are also included

Melt	Crystal	Denotation	$k_{eff\ Gd/Lu}$
Composition of LGSO:Sm^{3+}			
$(Lu_{0.500}Gd_{0.495}Sm_{0.005})_2SiO_5$	$(Lu_{0.510}Gd_{0.416}Sm_{0.005})_2SiO_5$	50Lu–50(Gd+Sm)	0.82
$(Lu_{0.170}Gd_{0.825}Sm_{0.005})_2SiO_5$	$(Lu_{0.173}Gd_{0.814}Sm_{0.006})_2SiO_5$	17Lu–83(Gd+Sm)	0.97
$(Lu_{0.150}Gd_{0.845}Sm_{0.005})_2SiO_5$	$(Lu_{0.130}Gd_{0.769}Sm_{0.009})_2SiO_5$	15Lu–85(Gd+Sm)	1.05
Composition of LGSO:Dy^{3+}			
$(Lu_{0.768}Gd_{0.192}Dy_{0.04})_2SiO_5$	$(Lu_{0.799}Gd_{0.163}Dy_{0.038})_2SiO_5$	76.8Lu–23.2(Gd+Dy)	0.82
$(Lu_{0.576}Gd_{0.384}Dy_{0.04})_2SiO_5$	$(Lu_{0.634}Gd_{0.331}Dy_{0.035})_2SiO_5$	57.6Lu–38.4(Gd+Dy)	0.78
Composition of LGSO:Ce^{3+}			
$(Lu_{0.495}Gd_{0.495}Ce_{0.01})_2SiO_5$	$(Lu_{0.568}Gd_{0.4235}Ce_{0.0036})_2SiO_5$	49.5Lu–50.5(Gd+Ce)	0.75
$(Lu_{0.10}Gd_{0.89}Ce_{0.01})_2SiO_5$	$(Lu_{0.0865}Gd_{0.915}Ce_{0.00635})_2SiO_5$	10Lu –90(Gd+Ce)	1.19

crystals. For comparison, the data reported for the LGSO:Dy [10] and LGSO:Ce [8] are presented also. The segregation properties between gadolinium and lutetium were determined along the growth direction of solid solution single crystal grown from the melt with composition $(Lu_{0.500}Gd_{0.495}Sm_{0.005})_2SiO_5$. The crystal boule was cut on slices and those from the beginning and the end were used to determined the concentration of components. The relation

$$C_s = k_{\text{eff}} * C_0 * (1-g)^{\text{keff}-1} \quad (1)$$

where k_{eff} is the effective distribution coefficient, C_0 is a starting component concentration in the melt, C_S means the concentration in crystal composition, and g represents the ratio of the crystal mass to the total starting mass in the crucible, was used to estimate the k_{eff} value. The effective segregation coefficient of the Gd/Lu in $(Lu_x Gd_{0.995-x}Sm_{0.005})_2SiO_5$ solid solutions is about $k_{\text{eff}}=0.82\pm0.04$ for $0.17<x<1$, and is reciprocal to the Lu/Gd segregation in LGSO ($k_{\text{eff}}=1.22\pm0.04$).

Reported data imply that in LGSO crystals rare earth dopants with ionic radii greater than ionic radius of Gd^{3+} (e.g. Ce^{3+}, Pr^{3+}, Sm^{3+}) replace gadolinium in crystal lattice [8],whereas, ions with smaller radii (e.g. Dy^{3+}) substitute site positions of lutetium ions [10]. It was shown that there is a linear dependence between the segregation coefficient of dopant (D) and an difference of ionic radii between cation (r_C) building the host and dopant (r_D) [8,11,12]. According to the equation proposed by Brandle et. al [11], a segregation coefficient (k_{eff}) is greater than unity when $r_C > r_D$. Otherwise, $k_{\text{eff}}<1$ for $r_C<r_D$. This tentative equation is satisfied when the C2/c-type lattice (LSO) is doped with Ce^{3+}, Sm^{3+}, Gd^{3+}or Dy^{3+}. It should be noted here that an increase of ionic difference ($r_C - r_D$), leads to the decreasing of segregation coefficient ($k_{\text{effCe}}<k_{\text{effSm}}<k_{\text{effGd}}<k_{\text{effDy}}$). However, this rule is correct only as far as the amount of admixture in crystal does not change its structure type. Table 1 reveals changes of segregation coefficients versus crystal compositions that indirectly can imply the structural phase transition from the C2/c- to the $P2_1/c$-type structure corresponding to the LSO and GSO crystals, respectively. On the basis of nominal and real compositions of the LGSO systems we can notice that the Lu/Gd ratios in crystals are higher than those in melts for the Lu^{3+} amount higher than 17 at% and, decrease for lutetium concentration lower than 17 at%. As a result, the Lu/Gd ratio becomes smaller than unity indicating the phase transition from the C2/c- to $P2_1/c$-type occurring in the LGSO matrix. A similar observation were reported for the $(Lu_{1-x}Gd_x)_2SiO_5$:Ce solid solutions [8] with $x=0.2$, 0.5, 0.9, and for the $(Gd_{1-x}Yb_x)_2SiO_5$ system [16]. It was reported that LGSO:Ce (90 at% of Gd) and GSO:Yb (10 at% of Yb) systems crystallize in $P2_1/c$ structure (such as LGSO with less than 16 at% of Lu). Moreover, the segregation coefficient of Yb^{3+} in GSO:Yb, estimated from the Yb^{3+} concentration in the crystal and the melt, was found to be smaller than unity ($k_{\text{effYb}}\approx0.86$). This value is in accordance with values observed for systems under study.

On the basis of the melt and crystal compositions and their melting temperatures, the schematic phase diagram was specified and presented in Fig. 1. Concentrations of Gd_2SiO_5 and Lu_2SiO_5 (in mol%) can be treated as components of solid solutions instead of constituent oxides (silicon oxide and rare-earth oxides). In the inset, the 0–25 mol% range is presented in greater details. Data presented for $x>0.5$ relate to those determined previously by us for the LGSO:Dy system [10]. Presented data clearly imply that the $(Lu_xGd_{1-x})_2SiO_5$ solid solution undergoes phase transition for $0.15<x<0.17$. Earlier studies on $(Lu_xGd_{1-x})_2SiO_5$ did not give an unequivocal answer to the Lu/Gd ratio being a crucial for the C2/c (LSO)→$P2_1/c$ (GSO) phase transition. Loutts et al. [8] have reported that the $(Lu_{1-x}Gd_x)_2SiO_5$:Ce crystals with $x\geq0.5$ and $x=0.9$ belong to the C2/c and $P2_1/c$ structure, respectively. Polymorphism in the LGSO:Ce solid solutions was also considered by Sidletskiy et al. [17]

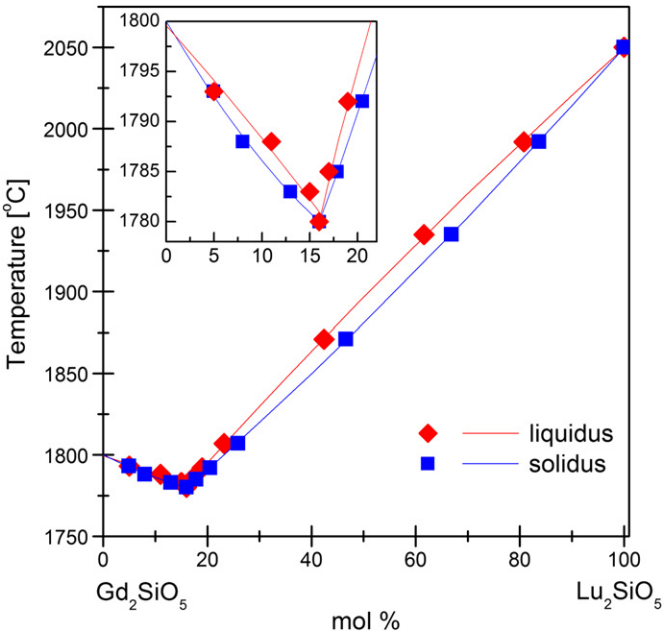

Fig. 1. Schematic phase diagram for Gd_2SiO_5–Lu_2SiO_5 solid solutions.

in the term of the Lu/(Lu+Gd) ratio. It has been shown that an increase of Gd^{3+} content in LGSO lattice results in the transformation of the C2/c structure into $P2_1/c$ one. Moreover, when the $Lu/(Lu+Gd)\leq0.1$ the solid phase is $P2_1/c$ whereas, when $Lu/(Lu+Gd)>0.2$ crystal grows in C2/c structure, irrespective of the type of used seed ([0 1 0] for GSO or [2 1 0] for LSO). Crystals with a symmetry of seed used in the melts grow in the range of $0.1<Lu/(Lu+Gd)<0.2$. Structural data reported for the $(Lu_{0.220}Gd_{0.740}Dy_{0.039})_2SiO_5$ crystal still keeping the C2/c structure even for almost 80% of Gd^{3+} in LSO lattice [10], confirm results considered above.

To avoid influencing of seeding on crystal structure, we used an iridium rod as a seed for growth of the $(Lu_xGd_{0.995-x}Sm_{0.005})_2SiO_5$ crystals. The phase formation was analyzed by X-ray diffractometry. Fig. 2 presents diffraction patterns of $(Lu_xGd_{1-x})_2SiO_5$ with $x=0.15$ and 0.17 in the melt. Presented patterns, differing in location, number, and intensity of diffraction lines, indicate that the samples are characterized by different crystallographic structure. It was found that solid solution crystals with $x\geq0.17$ (19, 35 and 50% of Lu^{3+}) belong to the LSO-type structure (C2/c) whereas, crystals with $x\leq0.15$ (11 and 9.5% of Lu^{3+}) have the GSO structure ($P2_1/c$). Presented data have proved that Lu^{3+} concentration in the melt is a crucial factor for the structural phase transition in LGSO:Sm system occurring for melt composition with x lower than 0.17 and higher than 0.15.

Table 2 depicts values of lattice constants and unit cell volume determined for the $(Lu_xGd_{1-x}Sm_{0.005})_2SiO_5$ solid solutions. It should be noted here that all data relate to crystalline hosts because the concentration of Sm^{3+} (only 0.5 at.%) is irrelevant for structural changes. As was expected, the phase formation reflected in structural parameters. The variations of structural parameters are graphically presented in Fig. 3 together with those reported for LGSO:Dy [10], for the data fullness. Table 3 contains structural and physical parameters describing the $(Lu_xGd_{0.995-x}Sm_{0.005})_2SiO_5$ crystal with $x=0.15$ and 0.17. Further details of the crystal structure investigations may be obtained from Fachinformationszentrum Karlsruhe, 76344 Eggenstein–Leopoldshafen, Germany (fax: (+49)7247-808-666; e-mail: crysdata(at)fiz-karlsruhe.de, http://www.fiz-karlsruhe.de/request_for_deposited_data.html) on quoting the appropriate CSD numbers – 423749 (LGSO:Sm $x=0.15$) and 423750 (LGSO:Sm $x=0.17$).

3.2. Raman study.

In order to determine both the symmetry of experimentally observed Raman-active modes and their assignment, the factor group analysis for appropriate structures of investigated crystals is required. Additionally, the set of polarized Raman spectra recorded in different scattering configurations has to be collected.

As was shown in Table 3, unit cells of LSO and GSO crystals contain 8 and 4 formula units, respectively. However, the primitive cell of both compounds contains four formula units ($Z_p=4$). Using the above assumption, Voron'ko et al. [18] have been presented calculations of zone center phonons. The 96 vibrational modes are distributed as follows:

$$\Gamma = 24A_g + 24B_g + 24A_u + 24B_u \quad (2)$$

Among them, 48 ($24A_g+24B_g$) are Raman-active modes. It is worth noticing that in a few previous papers [19–21] the authors performed the group theory calculations for the unit cell of LSO with eight formula units, and they obtained an incorrect irreducible representation given by following formula $48A_g+48B_g+48A_u+48B_u$. In order to predict correctly the number of vibrational modes for crystal, a primitive cell has to be taken into account.

The vibrational spectra of $(Lu_xGd_{0.995-x}Sm_{0.005})_2SiO_5$ crystal with $x=0.15$ ($P2_1/c$ space group) and 0.17 ($C2/c$ space group) were analyzed using Eq. (2). Considering Raman tensor for the 2/m point group, six scattering geometries have to be chosen to detect all Raman-active A_g and B_g modes. The A_g and B_g modes are recorded in $x(yy)x$, $x(zz)x$, $z(xx)z$, $y(xz)y \equiv y(zx)y$, $x(yz)x \equiv x(zy)x$ and $z(xy)z \equiv z(yx)z$ scattering geometries, respectively. Raman spectra recorded for both crystals in scattering geometries mentioned above are presented in Fig. 4. Despite the fact that the analysis of these spectra indicates a leakage of polarization of the strongest modes to forbidden polarization, an unambiguous assignment of mode symmetry is possible. The wavenumbers, symmetries and assignment of vibrations in the Raman spectra for the 15(Lu)–85(Gd+Sm) and 17(Lu)–83(Gd+Sm) samples are presented in Table 4. It should be emphasized that there is less experimentally observed modes in Raman spectra of both crystals than predicted by group theory. It is important to note that

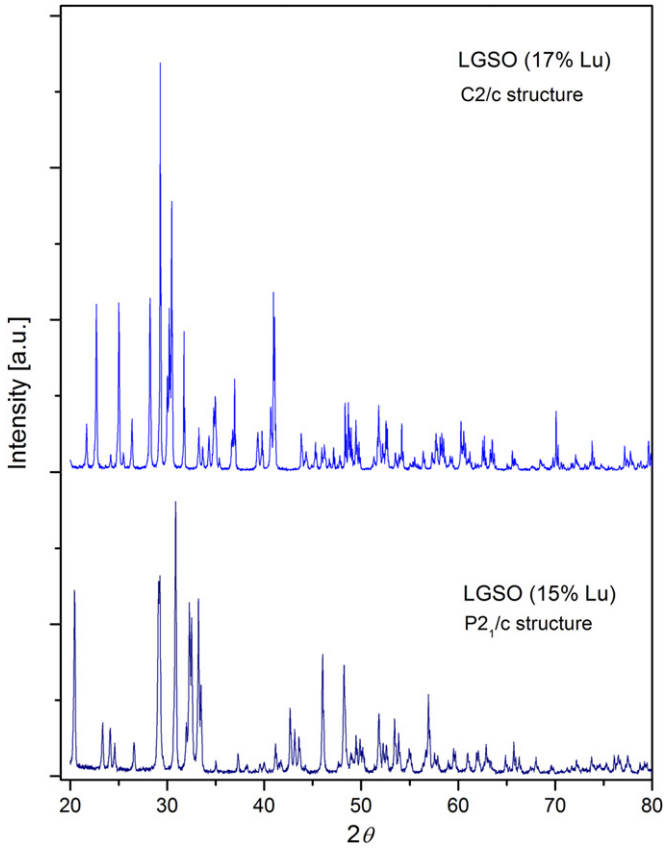

Fig. 2. X-ray diffraction patterns of the $(Lu_xGd_{1-x}Sm_{0.005})_2SiO_5$ solid solution crystals with $x=0.15$ and 0.17 in the melt.

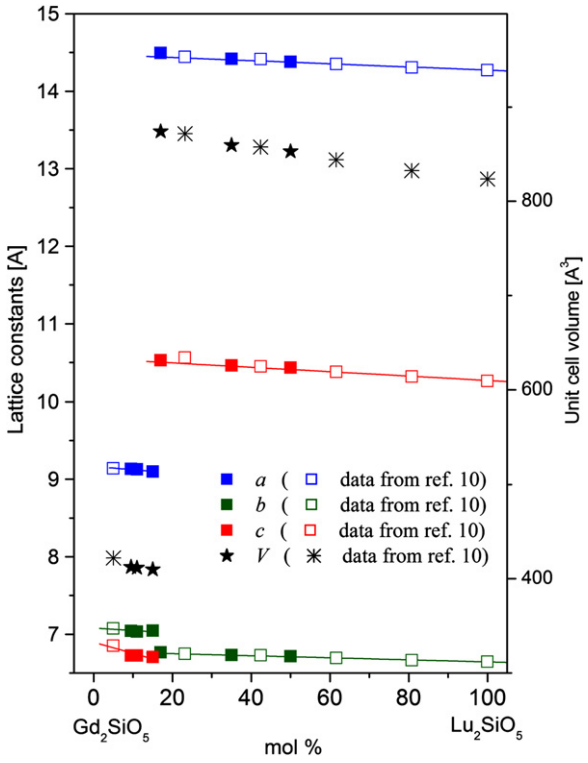

Fig. 3. Variations of lattice constants and unit cell volume determined for Gd_2SiO_5 – Lu_2SiO_5 system versus Lu^{3+} concentration in $(Lu_xGd_{1-x})_2SiO_5$ solid solution crystals.

Table 2
Rietveld refinement results for $(Lu_xGd_{1-x}Sm_{0.005})_2SiO_5$ crystals – space group, lattice constants (a, b, c, β), and unit cell volume (V)

Melt composition	Space group	Unit cell parameters (Å)				
		a	b	C	β	V (Å^3)
9.5Lu–90.5(Gd+Sm)	$P2_1/c$	9.1321(2)	7.0425(1)	6.7262(5)	107.55(4)	412.44(5)
11Lu–89(Gd+Sm)		9.1262(1)	7.0342(7)	6.7232(4)	107.52(3)	411.57(3)
15Lu–85(Gd+Sm)		9.1175(3)	7.0060(4)	6.7247(4)	107.44(8)	409.79(8)
17Lu–83(Gd+Sm)	$C2/c$	14.4947(6)	6.7669(8)	10.5284(5)	122.17(9)	874.04(9)
19Lu–81(Gd+Sm)		14.4540(8)	6.7526(9)	10.5593(3)	122.14(5)	872.64(9)
35Lu–65(Gd+Sm)		14.4169(6)	6.7325(7)	10.4617(2)	122.18(8)	859.43(5)
50Lu–50(Gd+Sm)		14.3794(9)	6.7148(4)	10.4312(6)	122.14(9)	852.80(4)

Table 3
Structural and physical parameters of $(Lu_xGd_{0.995-x}Sm_{0.005})_2SiO_5$ solid solution crystals with $x=0.15$ (GSO-type structure) and 0.17 (LSO-type structure).

Melt composition	$(Lu_{0.15}Gd_{0.845}Sm_{0.005})_2SiO_5$	$(Lu_{0.17}Gd_{0.825}Sm_{0.005})_2SiO_5$	
Crystal composition	$(Lu_{0.13}Gd_{0.865}Sm_{0.005})_2SiO_5$	$(Lu_{0.19}Gd_{0.805}Sm_{0.005})_2SiO_5$	
Space group setting	$P2_1/c$	$C2/c$	
Crystallographic system	Monoclinic		
Structure type	Triplite		
SG number	14	15	
Z number	4	8	
R_{wp} value	0.077	0.035	
Density (g cm^{-3})	6.54	6.55	
Melting point (K)	2057	2060	
Interatomic distance (Å)	Gd–O	Lu–O	
Gd1–O1	2.249(9)	Lu1–O5	2.203(4)
Gd1–O2	2.314(3)	Lu1–O1	2.300(2)
Gd1–O5*	2.328(2)	Lu1–O3	2.318(6)
Gd1–O4	2.388(6)	Lu1–O1	2.340(2)
Gd1–O2	2.470(7)	Lu1–O2	2.377(5)
Gd1–O1	2.485(6)	Lu1–O5	2.389(9)
Gd1–O2	2.532(2)	Lu1–O2	2.665(7)
Gd1–O4	2.662(9)		
Gd1–O4	2.734(2)		
Gd2–O5*	2.272(7)	Lu2–O5	2.209(2)
Gd2–O5*	2.277(7)	Lu2–O2	2.279(2)
Gd2–O5*	2.280(6)	Lu2–O4	2.279(8)
Gd2–O3	2.358(8)	Lu2–O4	2.279(9)
Gd2–O1	2.375(7)	Lu2–O3	2.236(4)
Gd2–O3	2.477(7)	Lu2–O5	2.306(8)
Gd2–O3	2.507(4)		
Gd1 –Gd1	3.697(7)	Lu1 –Lu1	3.243(6)
Gd1 –Gd2	3.744(3)	Lu1 –Lu2	3.638(3)
Gd2 –Gd2	3.465(1)	Lu2 –Lu2	3.459(8)
Si O1	1.600(8)		1.454(1)
Si O2	1.628(2)		1.544(7)
Si O3	1.629(2)		1.693(6)
Si O4	1.629(5)		1.949(3)
(Coordination number), *point symmetry*			
Gd1	(9), C_{3v}	Lu1	(7), C_1
Gd2	(7), C_s	Lu2	(6), C_1
Occupancy factor SOF	1 both for Gd1 and Gd2	1 both for Lu1 and Lu2	

* Relates to non-silicon-bonded oxygen.

our system configuration is not able to record Raman spectra below 100 cm^{-1} due to the edge filter cutoff. A few modes below 100 cm^{-1} have been registered for LSO and GSO compounds [18]. Taking those modes into account, a number of experimentally observed lattice modes in the LGSO systems is still less then theoretically predicted. On the basis of data presented in Table 4, Raman spectra of the LGSO:Sm solid solutions can be divided into three different regions, namely: (i) low-wavenumber range below 300 cm^{-1} which is connected with cation motions (lattice vibrations) and bending vibrations of SiO_4 tetrahedra, (ii) a range between 300–600 cm^{-1} related to RE–O stretching and SiO_4 bending vibrations, and (iii) high-wavenumber range between 800–1040 cm^{-1} in which SiO_4 symmetric and anti-symmetric stretching vibrations appear. Raman studies related to different orthosilicate systems (LSO, GSO, YSO, $(Lu_xY_{1-x})_2SiO_5$, Sc_2SiO_5) have shown that a part of the crystal vibrations can be identified with the internal motions of free SiO_4 tetrahedral ion. Referring to vibrations of isolated SiO_4 tetrahedron of point group symmetry T_d, its nine internal vibrations can be classified into four fundamental Raman-active modes: symmetric stretching vibration ν_1(A) (884 cm^{-1}), doubly degenerate bending vibration ν_2(E) (400 cm^{-1}), triply degenerate anti-symmetric stretching vibration $\nu_3(F_2)$ (905 cm^{-1}) and triply degenerate bending vibration $\nu_4(F_2)$ (559 cm^{-1}) [18,22].

The energy gap appearing in presented Raman spectra between 600 and 800 cm^{-1} is characteristic for compounds containing tetrahedral oxyanions [23]. Generally, this energy gap separates internal bending and stretching vibrations of tetrahedral molecules. However, in oxyorthosilicates in the range of bending vibrations, the stretching vibrations of RE–O bonds are recorded as well. Considering above noted deliberations, one can conclude that a detailed assignment of particular Raman modes in the spectral range below 600 cm^{-1} is very difficult.

Comparing polarized spectra of both crystals investigated we observe the separation of ν_4 bending modes appearing in the range of 500–600 cm^{-1}, from ν_2 bending and RE–O stretching modes in spectra of the 17Lu–83(Gd+Sm) crystal but no such separation is observed for the 15Lu–85(Gd+Sm). Raman modes recorded in the 315–400 cm^{-1} range, excluding the ν_2 bending mode at around 400 cm^{-1}, are assigned to RE–O stretching vibrations. Comparing Raman spectra of both samples in this spectral range, we observe the shift of modes to lower wavenumbers with the increase of Lu content in the sample. This shift is consistent with the increase of an average atomic mass of RE ions for sample 17Lu-83(Gd+Sm) in respect to sample 15Lu–85(Gd+Sm). A similar behavior was observed for modes appearing in the 100–250 cm^{-1} range, that can be connected with atomic mass of RE ions as well. The highest frequency of symmetric and asymmetric stretching vibrations of SiO_4 tetrahedra are recorded in the 850–1040 cm^{-1} and 880–990 cm^{-1} range for the 15Lu–85(Gd+Sm) and 17Lu–83(Gd+Sm) crystals,

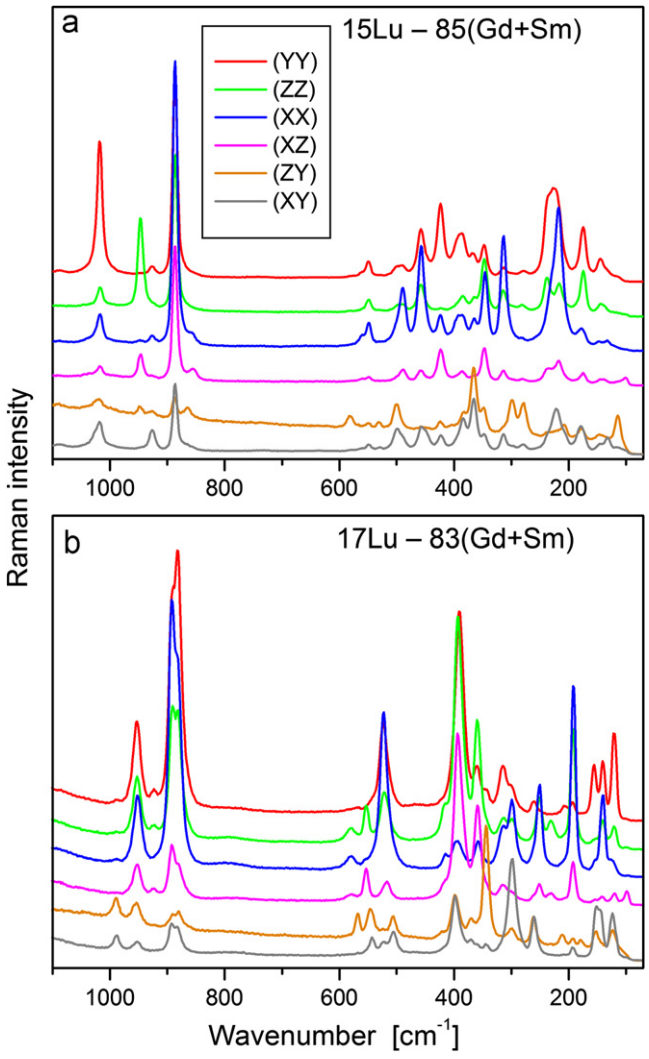

Fig. 4. Polarized Raman spectra of $(Lu_xGd_{0.995-x}Sm_{0.005})_2SiO_5$ crystal with $x=0.15$ (panel a) and $x=0.17$ (panel b) recorded in different scattering configurations.

Table 4
The wavenumbers, symmetries and assignment of Raman modes for $(Lu_xGd_{0.995-x}Sm_{0.005})_2SiO_5$ crystals with $x=0.15$ (15Lu–85(Gd+Sm)) and $x=0.17$ (17Lu–83(Gd+Sm)). Abbreviations T and L denote translatory and libratory modes, respectively.

wavenumber in cm^{-1} 15Lu –85(Gd+Sm)		17Lu–83(Gd+Sm)		Assignment
A_g	B_g	A_g	B_g	
	115		123	
		121		
	132			
144		140		
			145	
			153	
175		156		
	179		179	
	209		208	
217		192		
222			211	
235		230		T (RE)
		251		T, L (SiO_4)
	279		260	v (RE–O)
	299		299	v_2 (SiO_4)
314		315		
			344	
347		358		
	366		370	
384		391		
394		394		
			398	
424		418		
	450			
457				
491				
	500		506	
	531		545	
548		523		v_4 (SiO_4)
555		553		
		580		
	581		568	
856				
	865			
886		881		
		892		v_1, v_3 (SiO_4)
	926			
947		924		
1018		953		
	1026		990	

respectively. The number of experimentally observed modes in the region of stretching vibrations is lower for 17Lu-83(Gd+Sm) than for 15Lu–85(Gd+Sm). However, the splitting of the most intense symmetric stretching mode is observed only for the 17Lu-83(Gd+Sm) sample. Two components with maxima at 881 and 892 cm^{-1} are separated by 11 cm^{-1}. This value is significantly lower than those reported for the LSO (24 cm^{-1}) [20] and YSO (21 cm^{-1}) [22] crystals. For sample 15Lu–85(Gd+Sm) the symmetric stretching mode is observed at 886 cm^{-1} as a sharp single line. Presented structural studies revealed that phase transition occurs when the concentration of lutetium in the melt is higher than 15 and lower than 17 at.% (see Table 2). In crystal with $P2_1/c$ structure (15Lu–85(Gd+Sm) sample), SiO_4 tetrahedra are almost regular with comparable bond lengths within the range of 1.600–1.629 Å, and it is consistent with the observation of a single mode in Raman spectrum. However, the crystal with $C2/c$ space group (17Lu–83(Gd+Sm) sample), Si ions are tetrahedrally bonded to four oxygen atoms with two short bonds (1.454 and 1.544 Å) and two longer bonds (1.693 and 1.949 Å). Thus, in this structure tetrahedra are more distorted, and in consequence, the splitting of symmetric stretching v_1 vibration is observed in Raman spectrum. Room temperature Raman spectra of GSO, YSO and LSO compounds, belonging to the $P2_1/c$ (GSO), and $C2/c$ space groups (YSO, LSO), have been analyzed by Voron'ko et al. [18] paying special attention to regions of internal vibrations of SiO_4 tetrahedra, particularly the range of stretching vibrations. They have concluded that the structure of modes in this spectral range can be an useful tool for distinguishing between $P2_1/c$ and $C2/c$ crystallographic structure. Thus, oxyorthosilicates with $P2_1/c$-type structure should possess one strong feature in Raman spectrum in the range of stretching vibrations, whereas, for $C2/c$-type structure compounds a doublet of strong Raman modes should be observed. The results of Raman study obtained for 15Lu–85(Gd+Sm) and 17Lu–83(Gd+Sm) samples are entirely consistent with results discussed by Voron'ko et al. and allow us to distinguish between crystallographic structures of investigated samples. The phase transformation considered above can be caused either by change in the composition of solid solution or induced by pressure or temperature. On the evidence of this, the splitting of symmetric stretching mode could be observed in Raman spectrum. This phenomenon was reported for yttrium gadolinium oxyorthosilicate $Y_{2-x}Gd_xSiO_5$ compound [24] or lutetium yttrium oxyorthosilicate $Lu_{1.8}Y_{0.2}SiO_5$ crystals [21]. High temperature measurements for the 17Lu-83(Gd+Sm) solid solution, as a sample with lower symmetry described by $C2/c$, were carried out. Temperature evolutions of Raman spectra are presented in Fig. 5. For better presentation, the spectra were vertically shifted one to each other. All spectra were

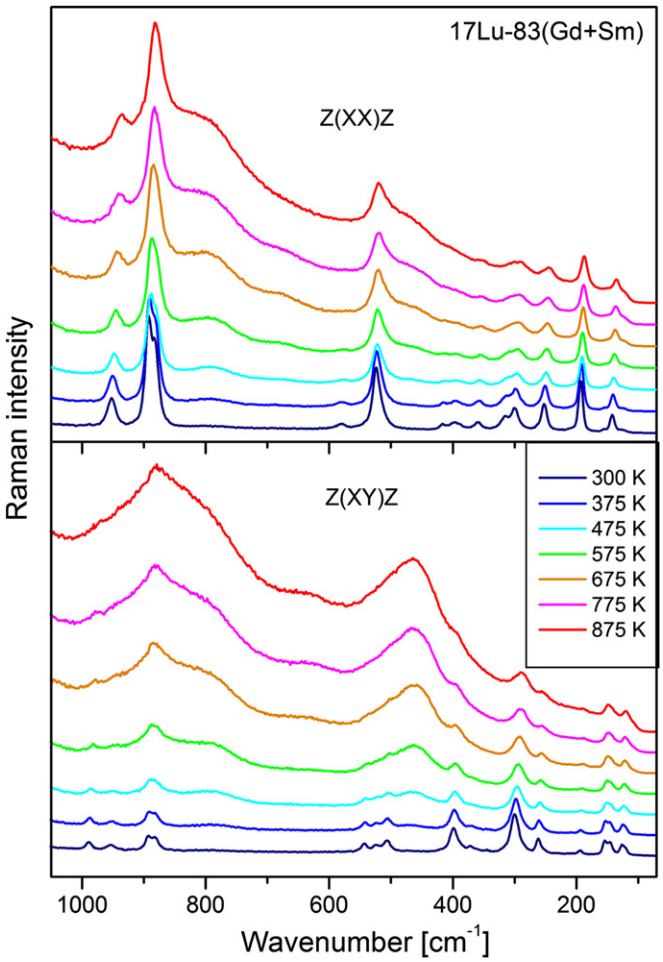

Fig. 5. Temperature evolutions of Raman spectra of the 17Lu-83(Gd+Sm) recorded in the *z*(*xx*)*z* and *z*(*xy*)*z* scattering geometry in the 300–875 K temperature range.

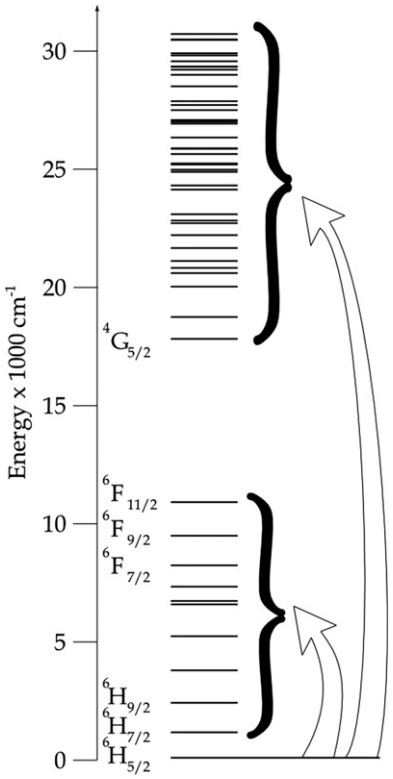

Fig. 6. Energy level diagram of Sm^{3+} ions in the LGSO solid solution crystal.

corrected with the Bose–Einstein population factor. The analysis of spectra revealed that the increase of temperature leads to the increase of Raman mode widths and the decrease of their intensity. It was found also that two components of symmetric stretching mode recorded at 881 and 892 cm^{-1} at room temperature merge into a single broad band when temperature increases (see *z*(*xx*)*z* scattering configuration). However, this effect can be due to broadening of these modes with increasing temperature giving the impression of mode character change. Raman modes are also overlapped by very broad bands with maximum at about 460 and 800 cm^{-1}, strongly increasing their intensity with temperature. These bands do not have vibrational origin and they are probably connected with luminescence properties of crystal. The observed shift of positions of Raman modes is caused by the lattice thermal expansion. Presented temperature date imply that the structure of $(Lu_{0.170}Gd_{0.825}Sm_{0.005})_2SiO_5$ solid solution crystal is rather stable up to 875 K, the highest temperature reached in our experiment. Thus, there is no arguments from Raman study for temperature-induced phase transition from C2/*c* to $P2_1/c$ in the temperature range being studied.

3.3. Optical properties

3.3.1. Samarium absorption and transition intensities.

Characteristic feature of absorption spectra of Sm^{3+} ions in LGSO matrix is the division of absorption bands into two groups. Absorption bands within first group occur in the near- and middle-infra-red region. They are related to transitions between the $^6H_{5/2}$ ground state and the $^6H_{7/2-15/2}$ and $^6F_{1/2-11/2}$ excited multiplets. A second group consists of numerous closely-spaced and usually overlapped multiplets in the region of 17 000–30 000 cm^{-1}. The scheme of energy levels with marked two groups of multiplets is shown in Fig. 6.

We hoped that structural peculiarity of the LGSO host will reflect in absorption and emission spectra of Sm^{3+} doped the matrix. Figs. 7 and 8 depict unpolarized absorption spectra of $(Lu_xGd_{0.995-x}Sm_{0.005})_2SiO_5$ solid solutions measured at 300 K for crystals with $x=0.5$, 0.19, 0.15, 0.11. Studied crystals are anisotropic. Therefore, to obtain meaningful data for the sake of comparison the measurement was performed with oriented sample plates having the same thickness, and with incident light propagating perpendicular to (0 0 1) crystal plane. It was found that the shape of spectral bands changes significantly between samples with $x=0.15$ and 0.19 and this change is clearly seen in the IR spectral region. It has been found also that absorption transitions in LGSO:Sm^{3+} system with the $P2_1/c$ structure (samples with $x=0.11$ and 0.15) are shifted toward lower energy with respect to the LGSO:Sm^{3+} system with C2/*c* structure (samples with $x=0.19$ and 0.50). Also, the number of visible band components in LGSO:Sm^{3+} with the C2/*c* structure is much greater. Absorption coefficients of bands registered in the 17 000–24 000 cm^{-1} range are very small and it becomes impossible to assign bands to transitions between individual multiplets. More intense absorption bands of Sm^{3+} ion are observed above 24000 cm^{-1}. This spectral range is dominated by intense band slightly bellow 25000 cm^{-1}. Well-defined maxima at 24 735 and 24 708 cm^{-1} are observed for the solid solutions with the $P2_1/c$ structure (11 and 15 at.% of Lu^{3+}). However, these absorption bands of the crystals with C2/*c* structure (19 and 50 at.% of Lu^{3+}) shows two narrow and intense band components peaking at 24 820 and 24 690 cm^{-1}. These transitions could be found useful for optical pumping by a blue diode laser for a possible laser generation. On the basis of absorption spectra, oscillator strengths

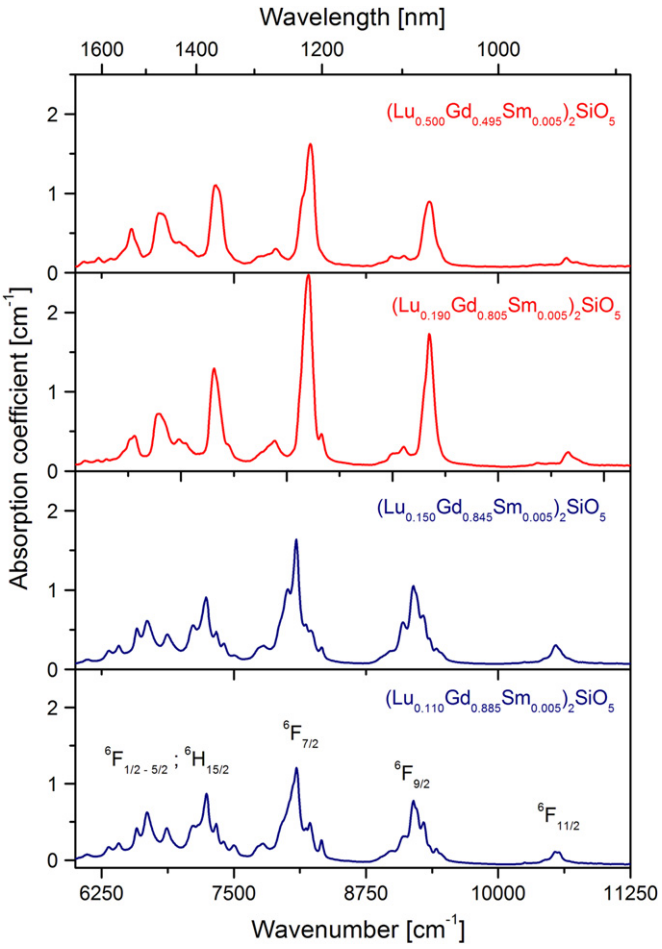

Fig. 7. Absorption spectra of the LGSO:Sm^{3+} crystals recorded at 300 K in the IR range.

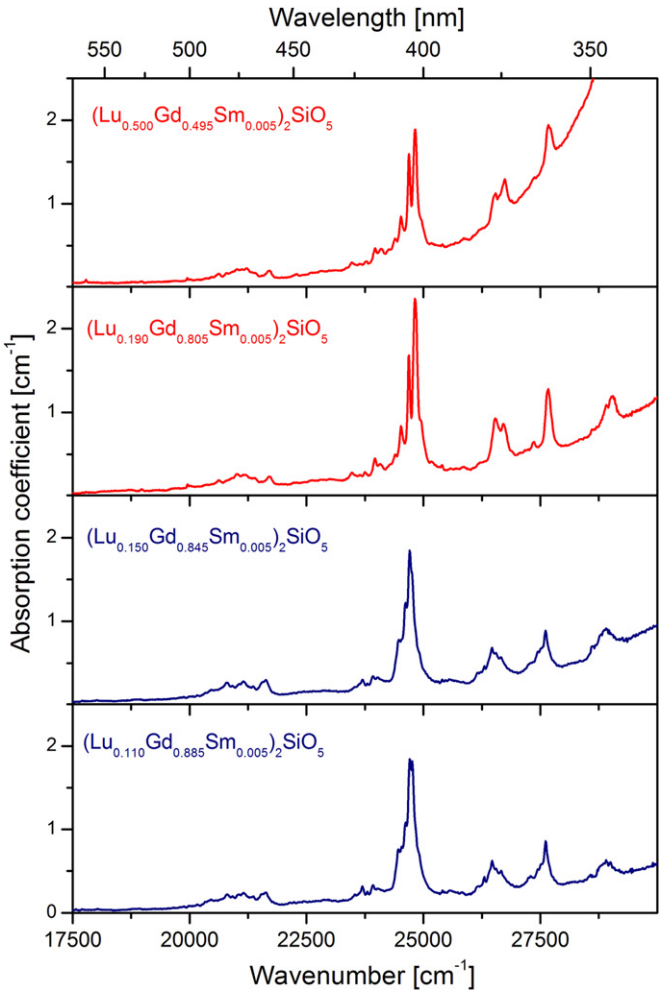

Fig. 8. Absorption spectra of the LGSO:Sm^{3+} crystals recorded at 300 K in the VIS range.

of transitions were calculated. The result is summarized in Table 5. Obtained values do not differ significantly. One can see also, that in the C2/*c* structure ascending admixture of Lu^{3+} amounts in $(Lu_xGd_{0.995-x}Sm_{0.005})_2SiO_5$ results in decreasing of experimentally calculated oscillator strengths.

3.3.2. Luminescent properties and excited state relaxation dynamics.

Fig. 9 shows unpolarized emission spectra of investigated crystals recorded under the 405 nm excitation. All measured the LGSO:Sm^{3+} samples show three emision bands originating from the $^4G_{5/2}$ excited state to the $^6H_{5/2}$, $^6H_{7/2}$ and $^6H_{9/2}$ levels. The spectra are dominated by band at around 600 nm. The maximum of this band appears at 600.3 nm for crystals with the C2/*c* structure and at 600.9 nm for crystals with the $P2_1/c$ structure. Effect of substitution of gadolinium by lutetium within the same type-structure on luminescence spectra is negligibly small. However, significant changes of emission spectra occur when the substitution of gadolinium by lutetium results in the change of the crystals structure from $P2_1/c$ to C2/*c*. Intensities of low- and high-energy band components in the transition from the $^4G_{5/2}$ state to the $^6H_{5/2}$ ground state are reversed. For the crystal with $x=0.19$, radiative transitions ending at lower-energetic components of the ground state are more intense whereas, for the crystal with $x=0.5$ the most intense transitions terminate at higher-energetic sublevels of the $^6H_{5/2}$ ground state. Such behavior is also evident in the case of the $^4G_{5/2}\rightarrow{}^6H_{9/2}$ luminescence. For the $^4G_{5/2}\rightarrow{}^6H_{7/2}$ transition both lower and higher energetic wings of the emission band are more intense for the crystal with $x=0.5$. The study shows that change of lutetium content in the crystal can induce the change of the shape of emission band.

All studied samples show single exponential luminescence decays although Sm^{3+} ions occupy two non-equivalent crystallographic positions in the two different structures of LGSO. This finding indicates that difference in the symmetry of the nearest surrounding of Sm^{3+} ions affects weakly rates of radiative transitions originating in the $^4G_{5/2}$ metastable level. This conclusion is corroborated by a similarity of experimental luminescence lifetime τ_{exp} values, gathered in Table 6.

4. Conclusions

The Sm^{3+}-doped $(Lu_xGd_{1-x})_2SiO_5$ solid solution single crystals with $x=0.095$, 0.11, 0.15, 0.17, 0.19, 0.35 and 0.5 were grown by the Czochralski method and their structural, physical and optical properties were investigated. On the basis of the variations of unit cell parameters, cell volume and melting temperature we imply that the break of the LSO to GSO structure occurs for solid solution composition with $0.15<x<0.17$. In LGSO solid solution crystals with $x\geq 0.17$, the Gd/Lu segregation coefficient $k_{effGd/Lu}$ is 0.82 but for crystal composition with $x\leq 0.15$, the $k_{effGd/Lu}$ is higher than unity. Raman scattering has been used to study Raman active phonons in solid solution crystals differing in

Table 5
Experimental oscillator strengths for $(Lu_xGd_{0.995-x}Sm_{0.005})_2SiO_5$ solid solution crystals with $x=0.11$, 0.15, 0.19 and 0.50. Center of the band was estimated using Gaussian fitting of shape of transition.

Multiplet	11Lu–89(Gd+Sm)		15Lu–85(Gd+Sm)		19Lu–81(Gd+Sm)		50Lu–50(Gd+Sm)	
	ν	f_{exp}	ν	f_{exp}	ν	f_{exp}	ν	f_{exp}
$^6F_{1/2}$; $^6F_{3/2}$; $^6H_{15/2}$; $^6F_{5/2}$	7 008	2.84	6 990	2.70	7 109	2.93	7 057	2.84
$^6F_{7/2}$	8 070	2.01	8 064	2.26	8 195	2.81	8 208	1.81
$^6F_{9/2}$	9 215	1.29	9 208	1.55	9 346	1.76	9 346	1.03
$^6F_{11/2}$	10 550	0.23	10 553	0.27	10 672	0.21	10 664	0.16
$^4G(4)_{7/2}$;$^4I(3)_{9/2}$; $^4M_{15/2}$; $^4I(3)_{11/2}$; $^4I(3)_{13/2}$	21 068	1.20	21 066	1.20	21 109	0.86	21 102	0.65
$^6P_{5/2}$, $^4M_{19/2}$; $^4L_{13/2}$; $^4F(3)_{7/2}$; $^6P_{3/2}$; $^4K(1)_{11/2}$; $^4M_{21/2}$; $^4L_{15/2}$; $^4G(4)_{11/2}$	24 735	4.41	24 708	4.07	24 820	4.44	24 820	3.10
$^4D(3)_{1/2}$; $^6P_{7/2}$; $^4L_{17/2}$; $^4K(1)_{13/2}$	26 515	0.95	26 506	0.89	26 610	1.14	26 649	0.80
$^4F(3)_{9/2}$; $^4D(2)_{3/2}$; $^6P_{5/2}$	27 587	0.88	27 569	0.76	27 670	0.97	27 682	0.54
$^4H(1)_{7/2}$; $^4K(1)_{15/2}$; $^4H(1)_{9/2}$; $^4K(1)_{17/2}$;$^6P_{7/2}$	28 896	0.45	28 874	0.70	28 993	0.74	29 002	0.47

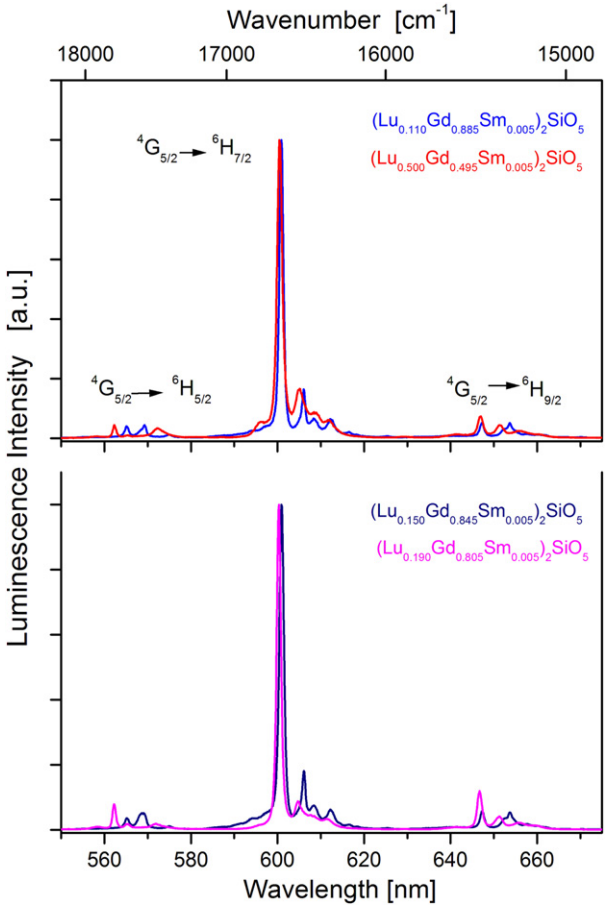

Fig. 9. Emission spectra of the $(Lu_xGd_{0.995-x}Sm_{0.005})_2SiO_5$ solid solution crystal with $x=0.11$ and 0.5 (upper picture) and $x=0.15$ and 0.19 (lower picture), normalized to the strongest band at about 600 nm. Crystals were excited into intense narrow line corresponding to the $^6H_{5/2}\rightarrow{}^6P_{3/2}$ transition ($\lambda_e x=405$ nm, $T=300$ K).

crystal structure. It was found that the replacement of Lu^{3+} by Gd^{3+} within one type of the crystal structure do not have a great influence on absorption and emission spectra. When structural phase transition occurs changes of emission band shape are significant. However, the rates of radiative and non-radiative transitions are similar for both crystal structures.

The $(Lu_xGd_{1-x})_2SiO_5$:Sm solid solution crystals offer an interesting alternative to Lu_2SiO_5 host for optical applications. Moreover, evaluated dependence of the melting temperature on the chemical composition of the systems under study indicates that an important advantage of solid solution crystals over Lu_2SiO_5 crystal stems from the fact that they can be grown at lower temperature and hence more easily and cheaply. Also, single crystals of LGSO possess better plasticity and lower tendency to crack.

Table 6
Experimental values of the $^4G_{5/2}$ lifetime of Sm^{3+} measured at 300 K.

	$(Lu_{0.11}Gd_{0.89})_2SiO_5$	$(Lu_{0.15}Gd_{0.85})_2SiO_5$	$(Lu_{0.19}Gd_{0.81})_2SiO_5$	$(Lu_{0.50}Gd_{0.05})_2SiO_5$
τ_{exp} (ms)	1.82	1.78	1.77	1.69

References

[1] J. Felsche, Struct. Bond. (Berlin) 13 (1973) 99–197.
[2] G. Anan'eva, A. Korovkin, T. Markulyaeva, A. Morozov, M. Petrov, I. Savinova, V. Startsev, P. Feofilov, Izvestiya AN SSSR, Neorg. Mater. 17 (6) (1981) 1037–1042.
[3] C.L. Melcher, J.S. Schweitzer, IEEE Trans. Nucl. Sci. NS. 39 (1992) 502–505.
[4] K. Takagi, T. Fukazawa, Appl. Phys. Lett. 42 (1983) 43–45.
[5] M. Korzhik, A. Fedorov, A. Annenkov, A. Borissevitch, A. Dossovitski, O. Missevitch, P. Lecoq, Nucl. Instrum., Methods Phys. Res. A 571 (2007) 122–125.
[6] W.W. Moses, Nucl. Instrum., Methods Phys. Res. A 487 (2002) 123–128.
[7] M. Jacquemet, C. Jacquemet, N. Janel, F. Druon, F. Balembois, P. Georges, J. Petit, B. Viana, D. Vivien, B. Ferrand, Appl. Phys. B: Laser Opt. 80 (2005) 171–176.
[8] G.B. Loutts, A.l. Zagumennyi, S.V. Lavrishev, Yu.D. Zavartsev, P.A. Studenkin, J. Cryst. Growth 174 (1997) 331–336.
[9] O. Sidletskiy, V. Bondar, B. Grinyov, D. Kurtsev, V. Baumer, K. Belikov, K. Katrunov, N. Starzhinsky, O. Tarasenko, V. Tarasov, O. Zelenskaya, J. Cryst. Growth 312 (2010) 601–606.
[10] G. Dominiak-Dzik, W. Ryba-Romanowski, R. Lisiecki, P. Solarz, B. Macalik, M. Berkowski, M. Głowacki, V. Domukhovski, Cryst. Growth Des. 10 (2010) 3522–3530.
[11] C.D. Brandle, A.J. Valentino, G.W. Berkstresser, J. Cryst. Growth 79 (1986) 308–315.
[12] C.L. Melcher, R.A. Manente, C.A. Peterson, J.S. Schweitzer, J. Cryst. Growth 128 (1993) 1001–1005.
[13] R. Lisiecki, G. Dominiak-Dzik, P. Solarz, W. Ryba-Romanowski, M. Berkowski, M. Głowacki, Appl. Phys. B: Laser Opt. 98 (2010) 337–346.
[14] G. Dominiak-Dzik, W. Ryba-Romanowski, R. Lisiecki, P. Solarz, M. Berkowski, Appl. Phys. B: Laser Opt. 99 (2010) 285–297.
[15] R.A. Young, A. Sakthivel, T.S. Moss, C.O. Paiva-Santos, J. Appl. Cryst. 28 (1995) 366–367.
[16] C. Yan, G. Zhao, L. Su, X. Xu, L. Zhang, J. Xu, J. Phys.: Condens. Matter 18 (2006) 1325–1333.
[17] O. Sidletskiy, V. Bondar, B. Grynyov, D. Kurtsev, V. Baumer, K. Belikov, Z. Shtitelman, S. Tkachenko, O. Zelenskaya, N. Starzhinsky, V. Tarasov, Crystallogr. Rep. 54 (2009) 1256–1260.
[18] Y.K. Voron'ko, A.A. Sobol, V.E. Shukshin, A.I. Zagumennyi, Y.D. Zavartsev, S.A. Koutovoi, Opt. Mater. 33 (2011) 1331–1337.
[19] S. Campos, A. Denoyer, S. Jandl, B. Viana, D. Vivien, P. Loiseau, B. Ferrand, J. Phys.: Condens. Matter 16 (2004) 4579–4590.

[20] D. Chiriu, N. Faedda, A.G. Lehmann, P.C. Ricci, A. Anedda, S. Desgreniers, E. Fortin, Phys. Rev. B 76 (2007) 1–8. 054112.
[21] P.C. Ricci, D. Chiriu, C.M. Carbonaro, S. Desgreniers, E. Fortin, A. Anedda, J. Raman Spectrosc. 39 (2008) 1268–1275.
[22] L. Zheng, G. Zhao, C. Yan, X. Xu, L. Su, Y. Dong, J. Xu, J. Raman Spectrosc. 38 (2007) 1421–1428.
[23] H.A. Szymanski, Raman Spectroscopy – Theory and Practice, Plenum Press, New York, 1967.
[24] J. Reichardt, M. Stiebler, R. Hirrle, S. Kemmler-Sack, Phys. Status Solidi A 119 (1990) 631–642.